Physics-informed data-driven reduced-order models for Dynamic Induction Control

Muscari, Claudia; Schito, Paolo; Viré, Axelle; Zasso, Alberto; van Wingerden, Jan Willem

DOI
10.1016/j.ifacol.2023.10.1036

Publication date
2023

Document Version
Final published version

Published in
IFAC-PapersOnLine

Available online at www.sciencedirect.com

ScienceDirect

IFAC PapersOnline CONFERENCE PAPER ARCHIVE

IFAC PapersOnLine 56-2 (2023) 8414–8419

Physics-informed data-driven reduced-order models for Dynamic Induction Control ⋆

Claudia Muscari [*,**] **Paolo Schito** [**] **Axelle Viré** [***] **Alberto Zasso** [**]
Jan-Willem van Wingerden [*]

[*] *Delft Center for Systems and control (DCSC), Faculty of Mechanical, Maritime and Material engineering, Technical University of Delft (Contact e-mail: claudia.muscari@polimi.it)*
[**] *Mechanical Department, Politecnico di Milano*
[***] *Wind Energy group, Faculty of Aerospace Engineering, Technical University of Delft*

Abstract: In this work, we find a reduced-order model for the wake of a wind turbine controlled with dynamic induction control. We use a physics-informed dynamic mode decomposition algorithm to reduce the model complexity in a way such that the physics of the wake mixing can be investigated and that the model itself can be easily embedded into control-oriented frameworks.
After discussing the advantage of forcing the linear system resulting from the algorithm to be conservative (as a consequence of the periodicity of the pitch excitation) and the choice of observables, we describe a procedure for calculating the energy associated with individual modes. The considered data-set is composed of large eddy simulation (LES) results for a single DTU 10 MW wind turbine in uniform flow. Simulations were performed first with baseline control (for reference) and then with the Pulse and the Helix approaches with constant excitation amplitude and different excitation frequencies. The frequencies and energies associated with the resulting modes are discussed.

Keywords: Wind Farm Control, Wake Mixing, Computational Fluid Dynamics, Dynamic Mode Decomposition, reduced-order Models

1. INTRODUCTION

As the installed wind energy capacity grows, both on-shore and off-shore, the general issue of how turbines influence the atmospheric boundary layer (ABL) and each other through it become more and more relevant. In a context where turbines are part of larger and larger wind farms and even those will be installed closer and closer together, any non-holistic approach to power maximization and blade load reduction (the two main objectives of wind farm control) will be sub-optimal.

This work focuses on Dynamic Induction Control (DIC), a flourishing new branch of wind farm control. The underlying idea is that time-varying control inputs can increase wake mixing and consequently improve the velocity recovery rate of the flow and the power production of downstream turbines.

The first instance of DIC, presented by Goit and Meyers (2015) relied on an unbounded optimal signal and was able, in numerical simulations, to increase power gains up to 21% with respect to greedy control. Munters and Meyers (2018), based on the observation that the optimal thrust coefficient signal in Goit and Meyers (2015) resembled a sinusoid, simplified the optimization problem significantly and reduced the detrimental effect on loads caused by a non-smooth control signal. In Frederik et al. (2020a), the sinusoidal variation of the thrust coefficient was obtained by exciting the collective pitch of the blades. This technique was called the Pulse because of the thrust magnitude variation's effect on the wake shape. The Helix (Frederik et al., 2020b) uses simple sinusoidal Individual Pitch Control (IPC) signals to impose yaw and tilt moments on the rotor and force wake meandering (Kimura et al., 2019). The strategy is called *helix* because it results in a helicoidal velocity field. If tilt and yaw angles have a phase offset equal to $\pi/2$, the Helix rotates in a counter clockwise (CCW) direction; if it is equal to $3\pi/2$, the Helix rotates in a clockwise (CW) direction. Preliminary tests show that the CCW-Helix leads to faster wake recovery than CW-Helix (Frederik et al., 2020b). This was confirmed in a recent study and it was found that the optimal signal frequency is equal to or higher than $St = 0.4$ for a signal amplitude of 4° (Muscari et al., 2022). The Strouhal number St, is often used in this context because it makes the analysis independent from the rotor diameter D and the free stream velocity U_∞.

The preliminary wind tunnel experiments (Frederik et al., 2020c) and numerical studies produced striking evidence of the potential of DIC, but further characterization of these techniques requires the development of reduced-order models (ROMs). We cannot possibly think of relying on large, computationally expensive, multiscale CFD simulations -let alone experimental campaigns! - in this explorative phase. Moreover, since the mixing mechanism is not clear yet, it would be helpful to isolate and observe the dominant structures in the wake. Although wakes are complex, high-dimensional, non-linear dynamical systems, they often exhibit low-dimensional behavior. In these cases, a data-driven perspective can complement more traditional model-based approaches. By applying modal decomposition techniques, we can represent the system with a number of modes orders of magnitude lower than the state dimension of the system.

⋆ This work was not supported by any organization

10.1016/j.ifacol.2023.10.1036

We chose to apply Dynamic Mode Decomposition (DMD), a data-driven technique native to the fluid-dynamics research community (Schmid, 2010). It is used to extract coherent patterns from high-dimensional flow data and obtain reduced-order models (ROMs) of the phenomena captured by the data. The modes and eigenvalues obtained are, in general, approximations of the ones of the Koopman operator, and the advantage with respect to proper orthogonal decomposition (POD) is the intrinsic temporal behavior associated with each mode. Also, because the modes are, in principle, non-orthogonal, they can sometimes be more physically meaningful than modes computed with POD.

These methods have been applied to wind turbine and wind farm flows in several forms and with various purposes. In Iungo et al. (2015), DMD is applied to actuator line (AL) simulations performed under uniform flow conditions and to actuator disk (AD) ones performed under turbulent flow. Sun et al. (2021) consider a two-bladed turbine and apply DMD on data from fully resolved CFD simulations in two different reference frames. In Cassamo and van Wingerden (2020), Input-Output Dynamic Mode Decomposition (IODMD) was used to derive a ROM for wake steering, and this was extended in Cassamo and van Wingerden (2021) with Koopman modes for wind farm control.

When we have some relevant information on the system's behavior, we can restrict the family of admissible data-driven models to a matrix manifold that respects the system's physical structure. A DMD algorithm with this constraint is called physics-informed (pi-DMD). In the case of DIC, Data-driven models of the wake flow could benefit from the periodicity of the pitch signals.

In this study, we apply conservative pi-DMD to large eddy simulation (LES) data of a single DTU 10 MW wind turbine in uniform flow, first with a baseline control (this will be our reference) and then with the Pulse and the Helix approach. To our knowledge, this is the first instance of a pi-DMD algorithm applied to DIC.

The remainder of this paper is structured as follows: Section 2 presents the theory behind pi-DMD following Baddoo et al. (2021), in Section 3 we describe the CFD simulations ran to produce the DMD snapshots. Finally, in Section 4 we analyze the results dedicating some space to the choice of observables (4.1) before diving into the energy analysis (4.2).

Since our objective was to investigate and explain the connection of frequencies and energies associated with the modes to the pitch excitation frequency, we defined a procedure for computing the energy of the individual modes and, thus, their contribution to the full reconstruction.

DMD proves to be a valid instrument for gathering a deep understanding of the physics of dynamically manipulated wakes as well as a simplified analytical model to embed in control-oriented frameworks such as FLORIDyn (Becker et al., 2022).

2. METHODOLOGY

In this section, we summarize the formulation of physics-informed DMD first presented in Baddoo et al. (2021) adapting it to our application.

2.1 Physics-informed DMD

DMD is definitely growing in popularity, but it has certain drawbacks that should be considered, the main two being a high sensitivity to noise and a tendency to over-fit.
Embedding physics into the learning framework can help in addressing these challenges. Let us suppose that we are studying a dynamical system defined by

$$X' \approx AX \qquad (x_{k+1} = Ax_k). \tag{1}$$

What DMD does is identify the best linear approximation of A. The matrices X and X' are built by collecting m snapshots of the considered flow field. For the particular case considered in this study, these state vectors are given by:

$$x_k = \left[u(t_k)^T \;\; v(t_k)^T \;\; w(t_k)^T \;\; p(t_k)^T\right]^T \in \mathbb{R}^{n\times 1}, \tag{2}$$

where $u(t_k)$, $v(t_k)$, $w(t_k)$ represent the vectorized velocity fields in the 3 dimensions at time instance t_k, and $p(t_k)$ contains the pressure field in the whole computational domain. We can organize the snapshots into the matrices X and X':

$$\begin{aligned} X &= [x_1 \;\; x_2 \;\; x_3 \;\; \dots \;\; x_{m-1}] \in \mathbb{R}^{n\times m-1}, \\ X' &= [x_2 \;\; x_3 \;\; x_4 \;\; \dots \;\; x_m] \in \mathbb{R}^{n\times m-1}, \end{aligned} \tag{3}$$

with $n \in \mathbb{Z}^+$ being the state dimension and $m \in \mathbb{Z}^+$ being the number of snapshots. The DMD problem can then be formulated as:

$$\underset{rank(A)=r}{\operatorname{argmin}} \|X' - AX\|_F. \tag{4}$$

where $||*||_F$ is the Frobenius norm. After approximately solving Eq. (4), the DMD process computes the dominant spectral properties of the learned linear operator. The rank-r constraint in Eq. (4) is motivated by the assumed modal structure of the system but does not account for other important physical properties.
For example, one limitation of DMD is that the solution of Eq. (4) lies within the span of X', so the learned model rarely generalizes outside the training regime. It is possible to incorporate physical principles into the optimization by constraining the solution matrix A to lie on a matrix manifold $\mathscr{M} \subseteq \mathbb{R}^{nxn}$:

$$\underset{A\subset\mathscr{M}}{\operatorname{argmin}} \|X' - AX\|_F. \tag{5}$$

The particular manifold $\mathscr{M}$ depends on the physical properties we want to enforce. The constraints make the learned model easier to generalize, reduce sensitivity to noise and reduce the demand for large training sets. The optimization problem given by Eq. (5) is known in the literature as a *Procrustes problem* and can be tackled as such.
A group of laws that can be easily incorporated into the DMD framework is conservation laws. Suppose that we are studying a system that we know conserves energy. In applications of DMD, it is implicitly assumed that measurements of the state have been suitably weighted so that the square of the 2-norm corresponds to the energy of the state: $E(x) = \|x\|_2^2$.
In these variables, the original optimization problems presented in Equations (4) and (5) equate to finding the model A that minimizes the energy of the error between the true and the predicted states (x_{k+1} and Ax_k, respectively). Thus, if A represents a discrete-time linear dynamical system ($x_{k+1} = Ax_k$), then A is an energy preserving operator, if and only if,

$$E(Ax) = \|Ax\|_2^2 = \|x\|_2^2 = E(x) \qquad \forall x \in \mathbb{R}^n \tag{6}$$

This means that A does not change the temporal energy of the system but merely redistributes energy between the states. Equation (6) holds, if and only if, A is *unitary*. This corresponds

to the orthogonal Procrustes problem. A will be constrained to be a unitary matrix, and the minimization problem will become:

$$\underset{A^*A=I}{\operatorname{argmin}} \|X' - AX\|_F \tag{7}$$

with solution, derived by Schönemann (1966):

$$A = U_{YX} V_{YX}^*, \tag{8}$$

where $U_{YX}\Sigma_{YX}V_{YX}^* = YX^*$ is a full singular value decomposition. The eigenvalues of A lie on the unit circle, and the eigenvectors are orthogonal. Thus, the eigenvectors oscillate in time with no growth or decay. Since the solution of the orthogonal Procrustes problem requires the full SVD of a $n \times n$ matrix, it can be more computationally efficient to first project onto the leading POD modes and build a model therein. In this case, the model is only energy preserving within the subspace spanned by the leading POD modes. The version of DMD that does this, with omitting the physics-informed step, is called *exact DMD*.

3. CASE SETUP

In this section, we describe the setup of the LES case used to build the data set. We ran a total of 9 simulations that only differed for the turbine control settings.

The DMD snapshots contained quantities extracted from LES performed in SOWFA (Churchfield et al., 2012) coupled to the super controller described in Fleming et al. (2013) to impose the sinusoidal pitching of the blades. The rotor is modeled with the Actuator Line Model (ALM), which substitutes the physical blades with body forces distributed along lines that represent them and the Atmospheric Boundary Layer (ABL) flow is governed by an incompressible formulation of the Navier-Stokes (NS) equations. The body forces, obtained through tabulated airfoil data, are projected back into the domain employing a three-dimensional smearing Gaussian function to prevent numerical issues. The main advantage of this kind of simulation is that it drastically reduces the computational cost while maintaining high-fidelity results. The inflow profile is uniform, with a wind speed at hub height equal to $9 m/s$ (below rated) to isolate the effect of the pitch actuation. The rotational speed is 7.12 rpm. Although these conditions are not representative of realistic working conditions in an actual wind farm, they are perfectly suited to visualize the effects of DIC on the wake.

The considered simulations employ the Pulse and counter clockwise Helix technique with different frequencies for the excitation, specifically $St = [0.2, 0.25, 0.3, 0.4]$, and a 4° amplitude. An additional simulation with baseline control is used as a reference. The considered rotor is the DTU 10 MW reference turbine (Bak et al., 2013), which has a diameter of $178.3 m$. The simulated time is $2000 s$ but, for our snapshots, we discard the transient part, corresponding to the initial $400 s$. The simulation time step is $0.2 s$ and a snapshot is taken once every $2 s$. The base mesh has the characteristics described in Table 1 and was locally refined to reach a characteristic cell dimension in the rotor area of $3.125 m$. The final number of cells is 9 millions. For the snapshots, we considered a sub-domain downstream of the rotor and further decimated the data in space by considering one out of four elements in x, y, and z. A fixed value of velocity and pressure is imposed at the inlet of the domain (west patch); velocity at the outlet (east patch) responds to the *inletoutlet* condition and to the slip condition on the remaining patches (lower, upper, south). The *inletoutlet* condition imposes a zero gradient of the quantity in general and a fixed value whenever backflow happens. The gradient of pressure is set to zero in the direction perpendicular to the patch for all patches except the inlet.

Table 1. Base mesh characteristics. Direction x is stream-wise, y is vertical, z is perpendicular to x and y.

	x	y	z
domain extension	2500 m	1000 m	600 m
number of cells	50	20	12

3.1 ALM optimal parameters

The requirements on the parameters imposed by the use of the ALM were respected: the projection function width was set to circa twice the characteristic cell dimension, i.e. $6m$. The choice of the correct value for this parameter is of the utmost importance. The reason is quite intuitive: if a very large value is chosen, the actuator line model will appear to recover an aerodynamic power exceeding the Betz limit, and if too small a value is chosen, the predicted power will be well below measurements or BEM calculations. The number of cells along a blade was higher than 50, which guaranteed an accurate description of the tip vortices.

4. RESULTS

In this section, after a brief detour on the topic of observables, we report the frequencies and energies associated with the obtained modes and discuss the results.

4.1 The choice of observables

When introducing DMD in Section 1 we said that the modes are approximations of the ones of the Koopman operator. The Koopman operator is an infinite dimensional linear operator that completely characterizes the dynamics of a nonlinear system. Its connection to DMD was first presented in Rowley et al. (2009), and it is strictly related to the notion of observable: a scalar-valued function of the state x. Intuitively we can think of them as the measurements we make. In section 2.1, we defined the state vector for our application as

$$x_k = \left[u(t_k)^T \;\; v(t_k)^T \;\; w(t_k)^T \;\; p(t_k)^T\right]^T \in \mathbb{R}^{n\times 1}, \tag{9}$$

The DMD performs a linear fit to the data coming from a nonlinear system. The conditions that must hold for DMD eigenvalues to be eigenvalues of the Koopman operator are discussed and proven in Tu (2013). A fundamental one is to have a sufficiently rich set of observables. Rowley and Dawson (2017) gives an extensive review of the topic and illustrates with an example how an incorrect choice of observables can lead us to draw false conclusions on the system dynamics. However, the procedure of choosing the observable is still addressed as an "art" rather than a science, which means that we decided to look at different combinations for the current study.

Table 2 shows the Strouhal numbers associated with the first seven modes obtained applying DMD to three different snapshot matrices: one containing only the measurements of the stream-wise component of the velocity, one containing all three and a third one accounting for the pressure as well. From our knowledge of the physics, we expect to find that the dominant modes are related to the DIC. They are indeed in all cases, but,

in the case where the full state vector is considered, some extra modes appear, clearly introduced by the pressure (considering the pressure only, leads to the same exact result).

Table 2. Strouhal numbers of the obtained DMD modes for the St=0.4 Helix simulation. DMD was performed on snapshots containing only the stream-wise velocity component, all three velocity components, and all tree velocity components plus pressure

	Strouhal		
	Only u	u,v,w	u,v,w,p
mode 0	0	0	0
mode 1	0.4	0.4	0.4
mode 2	0.8	0.8	0.8
mode 3	1.2	1.2	1.2
mode 4	1.6	1.6	1.454
mode 5	2	2	1.6
mode 6	2.4	2.4	2.841
mode 7	2.828	2.8	4.3181

Thus, when considering the full state vector, we will have mode 0, representative of the mean flow, mode 1 with the same Strouhal as the DIC excitation signal, modes 2,3 and 5 which are higher harmonics and what we can say about modes 6 and 7 is that, since their frequencies resemble respectively 1P and 2P they must be somehow related to the blade rotation around the stream-wise axis. This is confirmed by the fact that the frequencies of these modes vary only slightly with the Strouhal number for both Pulse and Helix cases and baseline as well. Table 3 shows the Pulse results and Figure 1 shows a reconstruction for the Helix case with St=0.2. It also reports energy

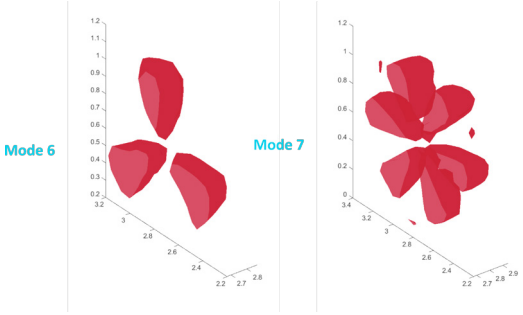

Fig. 1. Reconstruction of modes 6 and 7 represented via a convenient iso-surface of stream-wise velocity for the Helix case with $St = 0.2$. These modes appear when pressure is one of the observables.

values. The procedure for energy calculation will be presented in Section 4.2, but, for now, what matters that these values are not negligible, which means that we should ask ourselves whether they mean something or come from an incorrect choice of observables. Notice that, while in the example presented in Rowley and Dawson (2017), we could say that the choice of observables had lead to wrong results because we knew, a priori, what those results should look like; in this case, we do not have that knowledge. We will dismiss these additional modes for now, but the reason for their appearance should be investigated.

4.2 Energy analysis

The choice of the rank of our ROM is not as trivial as it would be with POD. POD modes are ordered based on their contribution to the main flow in terms of an energy computed as:

$$E = diag(S)^2. \tag{10}$$

The order of DMD modes should reflect their contribution to the flow field and separate relevant structures from noise-contaminated ones. There is no agreement in the literature on how to do that. In a previous work (Muscari et al., 2022) we converted the autonomous dynamic Equation (1) into its continuous time equivalent:

$$\frac{dx}{dt} = \tilde{A}_c x, \tag{11}$$

and took advantage of the physics of the system to get to a description of the flow from a given set of initial conditions $\alpha(t_1)$ at time instance t_1 into a response at time instance t_2 as a summation of modes:

$$\begin{bmatrix} u(t_2) \\ v(t_2) \\ w(t_2) \\ p(t_2) \end{bmatrix} = \Phi^{(0)}\alpha^{(0)}(t_1) + \sum_{i=1}^{q} \begin{bmatrix} \Phi_1^{(i)} & \Phi_2^{(i)} \end{bmatrix} \begin{bmatrix} \cos(\omega_i \Delta t) & \sin(\omega_i \Delta t) \\ -\sin(\omega_i \Delta t) & \cos(\omega_i \Delta t) \end{bmatrix} \begin{bmatrix} \alpha_1^{(i)}(t_1) \\ \alpha_2^{(i)}(t_1) \end{bmatrix}$$

with $\Delta t = t_2 - t_1$ and $\alpha_*^{(*)}(t_1)$ the initial condition of a corresponding mode at time instance t_1. The normalization of the mode shapes gives us the modal amplitudes:

$$\beta = \begin{cases} ||\Phi^{(0)}\alpha^{(0)}||_F & \text{for mode 0} \\ \sqrt{\left(\left|\left| \Phi_1^{(i)}\alpha_1^{(i)}(t_1) \right|\right|_F^2 + \left|\left| \Phi_2^{(i)}\alpha_2^{(i)}(t_1) \right|\right|_F^2 \right)} & \text{for the second order modes} \end{cases} \tag{12}$$

Following the approach commonly used for POD, we can relate the energy of a mode to the square of its mean modal amplitude. The results presented in this section refer to a snapshot matrix containing the three velocity components. Tables 4 and 5 show the frequencies of modes 0 to 7 and their energies normalized with respect to the energy of mode 0 for the baseline, for all St numbers considered and $r = 15$. The chosen rank gives a good trade-off between computational effort and energy retrieval.

Modes frequencies behave as expected for all of the Strouhal numbers. As we had done for Figure 1, we can plot iso-surfaces of stream-wise velocity reconstructed as $\Phi_1^{(i)}\alpha_1^{(i)}(t_1)$, where i is the number correspondent to the reconstructed mode. We use the information on the energy content for the choice of representative iso-values for the plot. We can recognize pulsating and helicoidal structures in correspondence with the excitation frequency and its integer multiples (Figure 2).

Let us now look back at either Table 4 or 5 to focus on the energy. The first thing we notice is how the baseline case could be reconstructed based on mode zero only, while, for the DIC cases, we would be losing around 1% of the total energy by doing that. Further comparison between the DIC cases and the baseline gives important insight into the accelerated recovery mechanism. Since the total energy is always higher for DIC cases than for the baseline, some of it is unequivocally introduced from the boundary layer. We already knew that mixing was at the base of the mechanism, but by looking at the energies of individual modes, we also see that it does not seem to be a redistribution of energy amongst the modes, which could also, in principle, be a part of the story. The effectiveness of DIC

Table 3. Frequencies and energies of the DMD modes 6 and 7 for the Pulse cases. The energy values are normalized with respect to the energy of mode 0 for the baseline. DMD was applied to full-state snapshots.

	Pulse St=0.2		Pulse St=0.25		Pulse St=0.3		Pulse St=0.4	
	Frequency	Energy	Frequency	Energy	Frequency	Energy	Frequency	Energy
mode 6	0.1355	0.005	0.1342	0.0049	0.1342	0.0048	0.1341	0.0051
mode 7	0.2293	0.0017	0.2311	0.0017	0.2326	0.0016	0.2329	0.0017

Table 4. Frequencies and energies of the obtained DMD modes for the Pulse simulations. The energy values are normalized with respect to the energy of mode 0 for the baseline.

	Baseline		Pulse St=0.2		Pulse St=0.25		Pulse St=0.3		Pulse St=0.4	
	Frequency	Energy	Frequency	Energy	Frequency	Energy	Frequency	Energy	Frequency	Energy
mode 0	0	1	0	1.02275	0	1.02455	0	1.02411	0	1.02194
mode 1	0.0339	0	0.01	0.00991	0.0125	0.01021	0.015	0.00983	0.02	0.00881
mode 2	0.0391	0	0.02	0.00364	0.025	0.0032	0.03	0.00268	0.04	0.00209
mode 3	0.0422	0.0001	0.03	0.00151	0.0375	0.00122	0.045	0.00107	0.06	0.00079
mode 4	0.0435	0	0.04	0.00075	0.05	0.0006	0.06	0.00055	0.08	0.00043
mode 5	0.0457	0	0.05	0.00046	0.0625	0.00038	0.075	0.00032	0.1	0.00023
mode 6	0.0835	0	0.06	0.00028	0.075	0.00023	0.09	0.00021	0.12	0.00012
mode 7	0.1399	0	0.0703	0.0002	0.0881	0.00015	0.1054	0.00014	0.1401	0
sum		1		1.039489		1.040544		1.038908		1.03449

Table 5. Frequencies and energies of the obtained DMD modes for the Helix and baseline simulations. The energy values are normalized with respect to the energy of mode 0 for the baseline.

	Baseline		Helix St=0.2		Helix St=0.25		Helix St=0.3		Helix St=0.4	
	Frequency	Energy	Frequency	Energy	Frequency	Energy	Frequency	Energy	Frequency	Energy
mode 0	0	1	0	1.023177	0	1.031096	0	1.035575	0	1.03767
mode 1	0.0339	0	0.01	0.010656	0.0125	0.011848	0.015	0.012123	0.02	0.011909
mode 2	0.0391	0	0.02	0.003103	0.025	0.003363	0.03	0.003425	0.04	0.003012
mode 3	0.0422	0.0001	0.03	0.001116	0.0375	0.001208	0.045	0.001131	0.06	0.000856
mode 4	0.0435	0	0.04	0.000474	0.05	0.00052	0.06	0.000489	0.08	0.000306
mode 5	0.0457	0	0.05	0.00026	0.0625	0.000245	0.075	0.000245	0,1	0.000138
mode 6	0.0835	0	0.06	0.000153	0.075	0.000138	0.09	0.000138	0,12	0
mode 7	0,1399	0	0.0703	0.000107	0.0881	0	0.1054	0	0.1401	0
sum		1		1.039045		1.048509		1.053202		1.053997

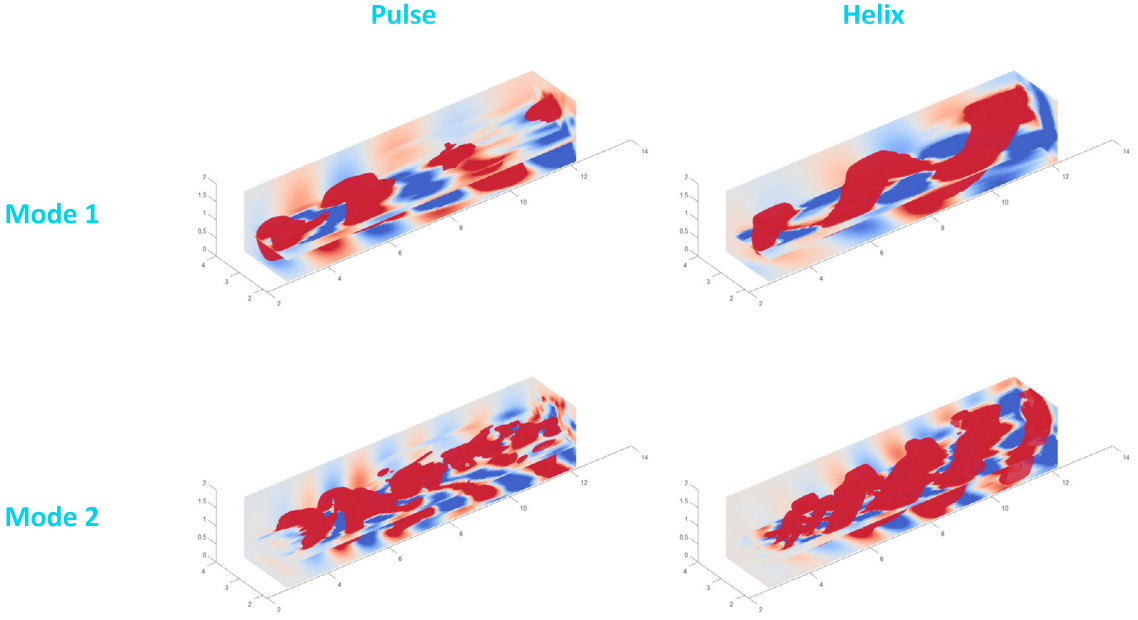

Fig. 2. Reconstruction of modes 1 and 2 represented via a convenient iso-surface of stream-wise velocity for the Pulse and Helix cases with $St = 0.2$

approaches is once more confirmed: previous evaluations of how it increases the energy content in the wake were done based on what was retrieved by a second turbine positioned downstream or by observing what was flowing through a selected plane parallel to the rotor one. The indication we get from mode 0, instead, is global. The Pulse still reaches an optimum for $St = 0.25$ and then the mean energy content decreases, for the Helix, until further studies, we can observe that it still increases for $St = 0.4$.

5. CONCLUSIONS

In this paper, we made a further step in characterizing the dynamic response of wakes manipulated with DIC techniques. We used a pi-DMD algorithm to force a conservative behavior of the obtained approximate linear systems. The data used to train the ROMs came from numerical simulations of the DTU 10 MW model turbine. Its operation under a uniform inflow was reproduced using the CFD framework SOWFA with the blades modeled as actuator lines.

We have shown how the choice of observables influences the results. By defining an energy associated with individual modes and comparing the results to a reference case with baseline control, we were able to generalize prior findings on both the Pulse and the Helix, such as the higher effectiveness of the latter at all excitation frequencies and the difference in optimal frequency.

The main conclusion of the work is that with DMD, we can obtain a ROM for dynamically controlled wake that can easily be embedded into control-oriented frameworks. In particular, from the energy evaluation, we see how one or two modes, in addition to mode 0, are sufficient to reconstruct the flow field appropriately. Emerging patterns in frequencies and energies for different excitation frequencies suggest that it might not be necessary to re-run CFD simulations and re-apply DMD for every change in conditions (flow and operating ones).

The analysis, for the Helix in particular, should be extended to higher St numbers and different excitation amplitudes. It is also our intention to apply the same pi-DMD procedure to experimental data. Finally, it is vital that all results are re-evaluated with a turbulent inflow.

REFERENCES

Baddoo, P.J., Herrmann, B., McKeon, B.J., Kutz, J.N., and Brunton, S.L. (2021). Physics-informed dynamic mode decomposition (pidmd). *arXiv preprint arXiv:2112.04307*.

Bak, C., Zahle, F., Bitsche, R., Kim, T., Yde, A., Henriksen, L., Hansen, M., Blasques, J., Gaunaa, M., and A, N. (2013). The DTU 10-MW reference wind turbine. In *Danish Wind Power Research 2013*.

Becker, M., Ritter, B., Doekemeijer, B., van der Hoek, D., Konigorski, U., Allaerts, D., and van Wingerden, J.W. (2022). The revised floridyn model: Implementation of heterogeneous flow and the gaussian wake. *Wind Energy Science Discussions*, 1–25.

Cassamo, N. and van Wingerden, J. (2020). On the potential of reduced order models for wind farm control: A koopman dynamic mode decomposition approach. *Energies*, 13(24). doi:10.3390/en13246513.

Cassamo, N. and van Wingerden, J. (2021). Model predictive control for wake redirection in wind farms: a koopman dynamic mode decomposition approach. In *2021 American Control Conf. (ACC)*, 1776–1782. IEEE.

Churchfield, M., Lee, S., and Moriarty, P. (2012). Overview of the simulator for wind farm application (sowfa). *National Renewable Energy Laboratory*.

Fleming, P., Gebraad, P., van Wingerden, J., Lee, S., Churchfield, M., Scholbrock, A., Michalakes, J., Johnson, K., and P, M. (2013). SOWFA super-controller: A high-fidelity tool for evaluating wind plant control approaches. Technical report, National Renewable Energy Lab.(NREL), Golden, CO (United States).

Frederik, J., Weber, R., Cacciola, S., Campagnolo, F., Croce, A., Bottasso, C., and van Wingerden, J. (2020a). Periodic dynamic induction control of wind farms: proving the potential in simulations and wind tunnel experiments. *Wind Energy Science*, 5(1), 245–257. doi:10.5194/wes-5-245-2020.

Frederik, J.A., Doekemeijer, B.M., Mulders, S.P., and van Wingerden, J.W. (2020b). The helix approach: Using dynamic individual pitch control to enhance wake mixing in wind farms. *Wind Energy*, 23(8), 1739–1751.

Frederik, J.A., Weber, R., Cacciola, S., Campagnolo, F., Croce, A., Bottasso, C., and van Wingerden, J.W. (2020c). Periodic dynamic induction control of wind farms: proving the potential in simulations and wind tunnel experiments. *Wind Energy Science*, 5(1), 245–257.

Goit, J.P. and Meyers, J. (2015). Optimal control of energy extraction in wind-farm boundary layers. *Journal of Fluid Mechanics*, 768, 5–50.

Iungo, G.V., Santoni-Ortiz, C., Abkar, M., Porté-Agel, F., Rotea, M.A., and Leonardi, S. (2015). Data-driven reduced order model for prediction of wind turbine wakes. In *Journal of Physics: Conference Series*, volume 625, 012009. IOP Publishing.

Kimura, K., Tanabe, Y., Matsuo, Y., and M, I. (2019). Forced wake meandering for rapid recovery of velocity deficits in a wind turbine wake. In *AIAA Scitech 2019 Forum*, 2083.

Munters, W. and Meyers, J. (2018). Towards practical dynamic induction control of wind farms: analysis of optimally controlled wind-farm boundary layers and sinusoidal induction control of first-row turbines. *Wind Energy Science*, 3(1), 409–425.

Muscari, C., Schito, P., Viré, A., Zasso, A., van der Hoek, D., and van Wingerden, J. (2022). Physics informed dmd for periodic dynamic induction control of wind farms. In *Journal of Physics: Conference Series*, volume 2265, 022057. IOP Publishing.

Rowley, C.W. and Dawson, S.T. (2017). Model reduction for flow analysis and control. *Annu. Rev. Fluid Mech*, 49(1), 387–417.

Rowley, C.W., Mezić, I., Bagheri, S., Schlatter, P., and Henningson, D.S. (2009). Spectral analysis of nonlinear flows. *Journal of fluid mechanics*, 641, 115–127.

Schmid, P.J. (2010). Dynamic mode decomposition of numerical and experimental data. *Journal of fluid mechanics*, 656, 5–28.

Schönemann, P.H. (1966). A generalized solution of the orthogonal procrustes problem. *Psychometrika*, 31(1), 1–10.

Sun, C., Tian, T., Zhu, X., Hua, O., and Z, D. (2021). Investigation of the near wake of a horizontal-axis wind turbine model by dynamic mode decomposition. *Energy*, 227, 120418.

Tu, J.H. (2013). *Dynamic mode decomposition: Theory and applications*. Ph.D. thesis, Princeton University.